Hindawi
Journal of Sensors
Volume 2020, Article ID 9231571, 10 pages
https://doi.org/10.1155/2020/9231571

Research Article

Dynamic Measurement of Legs Motion in Sagittal Plane Based on Soft Wearable Sensors

Yaqing Feng,[1] Yongze Li,[1] David McCoul,[2] Shihao Qin,[1] Tao Jin,[3] Bo Huang,[1] and Jianwen Zhao[1]

[1]*Department of Mechanical Engineering, Harbin Institute of Technology, Weihai 264209, China*
[2]*Department of Materials Science and Engineering, UCLA, Los Angeles, CA 90095, USA*
[3]*Department of Electronics Engineering, Harbin Institute of Technology, Weihai 264209, China*

Correspondence should be addressed to Bo Huang; huangbo74@163.com and Jianwen Zhao; zhaojianwen@hit.edu.cn

Received 29 October 2019; Revised 14 January 2020; Accepted 23 January 2020; Published 15 February 2020

Academic Editor: Marvin H Cheng

Human motion capture is widely used in exoskeleton robots, human-computer interaction, sports analysis, rehabilitation training, and many other fields. However, soft-sensor-based wearable dynamic measurement has not been well achieved. In this paper, the dynamic measurements of legs were investigated by using dielectric elastomers as stain sensors, and an alternating signal was applied to detect the dynamic rotational angles of the legs. To realize a quick response, parameters of the sensors were optimized by circuit analysis. The sensor can detect hip, knee, and ankle joint motions with a sample frequency of 200 Hz. The measurements of the sensors were compared with a commercial motion capture system from PhaseSpace, and dynamic errors between them were smaller than 3° when squatting and walking at low speed and smaller than 5° when walking at high speed. Experiments therefore demonstrate the feasibility of the integrated wearable stretch sensors with pants.

1. Introduction

Motion capture systems for tracking leg motion are widely applied in many fields, such as rehabilitation [1–3], competitive training [4], human-computer interaction [5], movie, animation [6], and exoskeleton assist systems [7]. The measurement of joint motion can ensure safe and effectual rehabilitation of leg motion [8]; several systems for leg rehabilitation have been developed that are applied to rehabilitation of spinal cord injury and neurological or orthopedic lesions [9–11]. In addition, the capture and analysis of joint motions can improve the competitiveness of some sports. For example, swimming requires proper leg posture to obtain optimal performance, and accurate feedback of leg motion can guide training for the sport [12]. Moreover, precise measurements of joint angles can make exoskeletons more comfortable.

The current measurement methods mainly include optical dynamic motion capture system based on vision technology [13], ultrasound based [14], electromagnetic based [15], linkage measurement based on mechanism, and IMUs (inertial measurement unit) [16, 17]. The first three methods require a system to generate a specialized peripheral signal, and the system cannot be fully integrated into the human body, so the first three methods are not applicable to measure the joint motions of mobile human body. The linkage measurement system is bulky and extremely inconvenient to wear. The inertial sensor obtains the angle value through integral operations, which can cause a large drifting. Therefore, soft strain sensor is a good candidate to measure the motion of human joint, because of its flexibility, comfort, compliance, low cost, and large strain.

The soft strain sensor mainly consists of a soft substrate and stretchable conductive electrodes. The general materials of the substrate are rubber [18–20], PDMS [21–24], cotton-based materials [25–27], etc.; the conductive electrode materials mainly include carbon black [28], carbon nanotubes [25], metal nanowires [29], and grapheme [30]; the

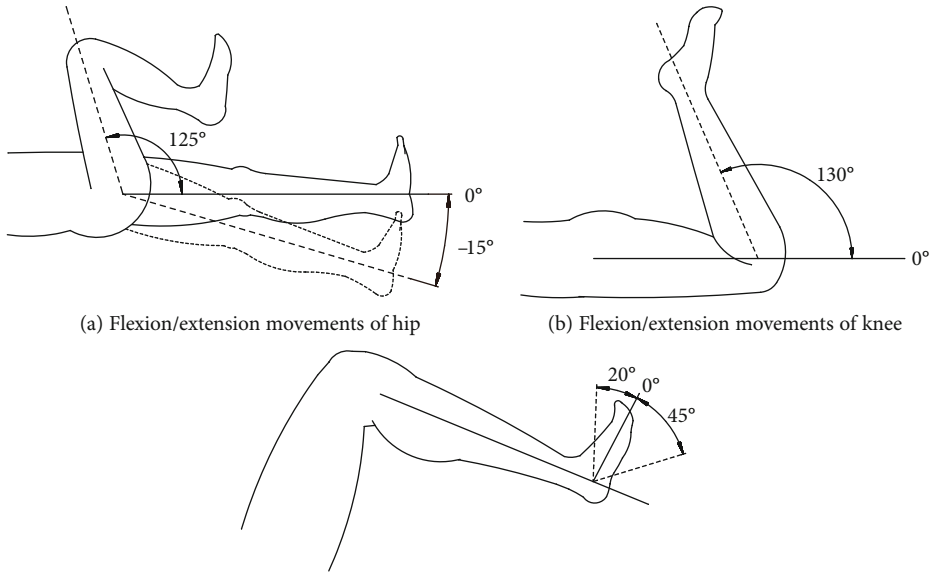

(a) Flexion/extension movements of hip

(b) Flexion/extension movements of knee

(c) Dorsiflexion/plantarflexion movements of ankle

Figure 1: Range of motion of the hip, knee, and ankle.

measurement principles include capacitance-based type and resistance-based type. Repeatability of the resistance-based type is not good, so high precision is hard to be guaranteed [20, 25]. Therefore, the capacitive strain sensor is more suitable for human motion measurement, and the capacitive soft sensor based on the dielectric layer of silicone rubber is more advantageous in terms of performance indicators, stability, and lifetime [31]. The group of Prof. Anderson has made significant progress with the dielectric elastomer sensor (DES) based on silicone rubber as applied to detect finger motion [32–34] and the leg motion of a diver [35], but the measurement errors are still high. Therefore, in this paper, we demonstrate the dynamic measurements of leg motion by utilizing optimized wearable DESs, and precision of the DESs is better than the published data of dynamic measurements [35–37].

2. Motion Analysis of Legs in Sagittal Plane and the Measurement Principle

Typical movements such as lifting and walking of the lower extremities mainly occur in the sagittal plane, including the pitching motion of the hips, knees, and ankles. When the human body stands in a neutral position, the hip joint performs flexion/extension in the sagittal plane around the frontal axis. The movement of the thigh to the front of the body has a flexion range of 0-125 degrees, and the backward movement has a range of 0-15 degrees, as shown in Figure 1(a). The knee joint performs flexion/extension in the sagittal plane with a range of 0 to 130 degrees, as shown in Figure 1(b). The ankle joint performs a dorsiflexion/plantarflexion movement in the sagittal plane around the frontal axis. The movement to the back of the foot is dorsiflexion with a range of 0 to 20 degrees. Movement to the sole is a plantar flexion with a range of 0 to 45 degrees.

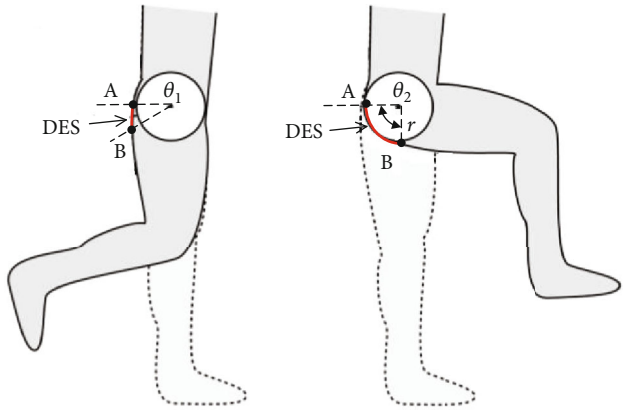

Figure 2: Stretching of the DES with rotation of the joint.

To measure the rotational angle of the hip, knee, and ankle joints, the soft strain sensors were mounted on these regions as diagrammed in Figure 2. The strain sensor was fixed to a pair of athletic pants at points *A* and *B*; the pants can deform with the rotation of the joints, and the strain sensor is sufficiently soft, so the distance between points *A* and *B* will vary. Relationship was determined between the rotation angle and the sensor strain, which is approximately linear if the strain sensor is suitably placed.

3. Design and Optimization of the Strain Sensor for Dynamic Measurements

Silicone has large stretchability and tensile strength, so silicone was chosen as the material of the dielectric layer of the strain sensor, and integrated silicone and carbon powder were chosen for the electrodes. The strain sensor consists of three layers of silicone membranes and two layers of electrodes, as shown in Figure 3(a). The middle layer is the

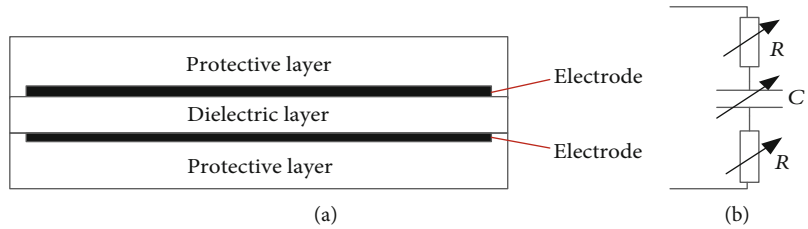

Figure 3: (a) Typical structure of a dielectric elastomer sensor (DES). (b) Equivalent circuit of the DES.

dielectric, while the outer layers are used for protection. The protective layers should cover the electrode areas and should also be as soft as possible so as not to restrict the deformation of the sensor. This DES structure creates an electrically flexible capacitor. The simplified equivalent electrical circuit is a variable capacitor C in a series with two variable resistors R to account for the resistance of the electrodes, as shown in Figure 3(b).

Both the capacitance and the resistance change with the deformation of the DES, and these changes can be used to infer the deformations. Compared to the series resistance, measuring changes in capacitance with deformation is more straightforward and reliable because the resistance is extremely dependent on the electrode uniformity and environmental temperature [38]. Capacitance of the DES can be calculated by Equation (1):

$$C = \frac{\varepsilon_0 \varepsilon_r A}{t} = \frac{\varepsilon_0 \varepsilon_r w l}{t} = \frac{\varepsilon_0 \varepsilon_r \xi_w w_0 \xi_l l_0}{\xi_t t_0}, \quad (1)$$

where ε_0 is the vacuum permittivity, ε_r is the relative permittivity of the dielectric layer material, A is the area of the overlapping electrodes, t is the thickness of the dielectric layer, w is the width of the electrode area, and l is the length of the electrode area. ξ_l, ξ_w, and ξ_t are strains of the length, width, and thickness, respectively, and ξ_w is equal to ξ_t because both directions are free of constraint. Therefore, Equation (1) can be simplified to

$$C = \frac{\varepsilon_0 \varepsilon_r w_0 l_0}{t_0} \xi_l. \quad (2)$$

From Equation (2), variations in the strain of the DES length can be linearly converted to variations in capacitance, and then we can detect the capacitance and calculate the DES length.

The principle of capacitance detection can be divided into frequency response-based methods, charge integration-based methods, and impedance matching-based methods, but these methods cannot balance detection speed and accuracy [33], so the principle of capacitance detection should be selected according to engineering requirements. Since the lower limb motion measurement requires a fast response, in this paper, a frequency-based method was applied: setting a sinusoidal voltage impulse (U_0 in Figure 4), and the sensor capacitance can be detected by variation of its voltage amplitude as shown in Figure 4. Here, C is the capacitance

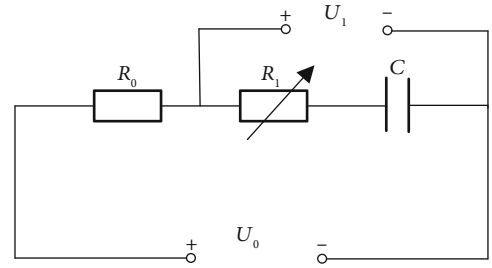

Figure 4: Soft sensor detection equivalent circuit schematic.

of the soft sensor, R_1 is the equivalent resistance of the soft sensor electrodes, R_0 is a setting constant resistance, U_0 is the sine wave excitation signal, and U_1 is the response signal to be collected.

The amplitude U_{1m} of the response signal U_1 can be derived as follows:

$$Z = R_0 + R_1 - \frac{1}{2\pi f C} j, \quad (3)$$

$$U_{1m} = \sqrt{U_{Cm}^2 + U_{Rm}^2} = \frac{\sqrt{(2\pi f C R_1)^2 + 1}}{\sqrt{[2\pi f C (R_1 + R_0)]^2 + 1}} U_{0m}, \quad (4)$$

where U_{0m} is the amplitude of the excitation signal U_0, U_{Cm} is the amplitude of the voltage of sensor, and U_{Rm} is the amplitude of the voltage of R_0. In the process of stretching the soft sensor, the capacitance and resistance of the sensor can be expressed by $C(t)$ and $R(t)$. Therefore, Equation (4) can be rewritten as

$$U_{1m} = \sqrt{U_{Cm}^2 + U_{Rm}^2} = \frac{\sqrt{(2\pi f C(t) R_1(t))^2 + 1}}{\sqrt{[2\pi f C(t)(R_1(t) + R_0)]^2 + 1}} U_{0m}. \quad (5)$$

The sensitivity of the DES can be calculated as Equation (6), where v is the stretching velocity of the sensor and k_v is the slope of U_{1m} during stretching.

$$s = \frac{\Delta U_{1m}}{\Delta l} = \frac{\boldsymbol{d} U_{1m} / \boldsymbol{d} t}{\boldsymbol{d} l / \boldsymbol{d} t} = \frac{k_v}{v}. \quad (6)$$

Table 1: Parameter variations of the DES with varying length.

Length l (mm)	Capacitance C (pF)	Resistance R_1 (kΩ)	Measuring voltage (mV)	Model voltage (mV)
65	664.8	10.5	1533	1530
70	708.2	11.7	1466	1466
75	751	12.3	1409	1409
80	796.6	13.4	1352	1350
85	843.7	14.4	1297	1294
90	891	15.4	1242	1241
95	941.2	16.3	1195	1188
100	990.3	17.5	1147	1140
105	1040	18.4	1100	1095
110	1090	19.6	1054	1053
115	1145	20.7	1015	1009
120	1197	21.9	975	971
125	1251	22.9	943	934
130	1304	24.0	906	901

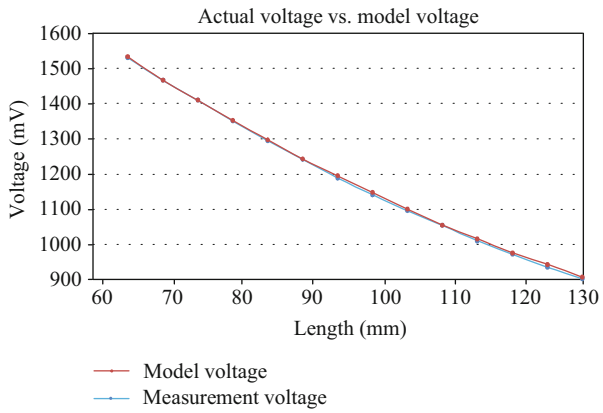

Figure 5: Comparison of experimental measurements and theoretical calculations.

When the DES is stretched at a constant speed, the capacitance of the sensor increases linearly and the voltage of the sensor decreases exponentially, so the instantaneous slope of U_{1m} decreases all the time. Therefore, in this approach, we use the average slope $(U_{1mo} - 0.8U_{1mo})/\Delta t$ to represent k_v, where U_{1mo} is the initial value of U_{1m} during stretching and Δt is the time when the U_{1m} drops to 80% U_{1mo}. As a result, Equation (6) can be replaced by Equation (7).

$$s = \frac{k_v}{v} = \frac{(U_{1mo} - 0.8U_{1mo})/\Delta t}{v}. \tag{7}$$

Parameters of the sensor measured by an LCR meter (Tonghui, TH26011BS) are shown in Table 1.

Figure 5 shows a good fit between the theoretical model of the sensor (Equation (4)) and the measured voltage of the sensor.

Fitting the data in Table 1, we can obtain Equation (8). Variation in capacitance and resistance of the sensor with the time during stretching are given in Equation (9), which is derived from Equation (8):

$$\begin{cases} C(l) = 9.87l + 9.80, \\ R_1(t) = 0.21l - 3.17, \end{cases} \tag{8}$$

$$\begin{cases} C(t) = 9.87vt + 664.8, \\ R_1(t) = 0.21vt + 10.5. \end{cases} \tag{9}$$

Sensitivity is the most significant parameter when the voltage amplitude is limited. From Equations (5) and (6), we know that all the parameters U_{0m}, R_0, and f will influence the sensitivity of the sensor, so they should be optimized. In this approach, we used a genetic algorithm to find the optimal solution because it has no limitation of step length and the stretch is fast. According to the performance characteristics of the microcontrollers and amplifier circuit, the optimum parameter range was set to $R_0 = 100\,\text{k}\sim1\,\text{M}\Omega$, $f = 200\sim1\,\text{kHz}$, and $U_{0m} = 0\sim3.3\,\text{V}$. (Specific parameter ranges can be selected according to specific conditions.) Their optimized values are shown in Table 2.

4. Placement of the DES and Integration of the DES with Pants

The system should measure the joint angle of the hip, knee, and ankle joints in the sagittal plane, so there are in total six degrees of freedom, including flexion/extension movements of the hip and knee joints and dorsiflexion/-plantarflexion movements of the ankle joint. The movement of the hip, knee, and ankle in the sagittal plane can be simplified to a hinge mechanism, and the joint angle can be simplified to the angle between the two parts of the limb in the sagittal plane.

The hip joint is composed of the femur and hip bone, as shown in Figure 6(a). The hip joint has three degrees of

Table 2: Optimized parameters of the sensor.

Signal amplitude U_{0m} (V)	Signal frequency f (Hz)	Series resistance R_0 (kΩ)	Sensitivity s (mV/mm)
3.3	932	317	33.2 (optimal value)
3.0	700	200	22.2
2.5	500	500	24.3
2.0	300	800	18.9
1.3	1000	1000	6.8

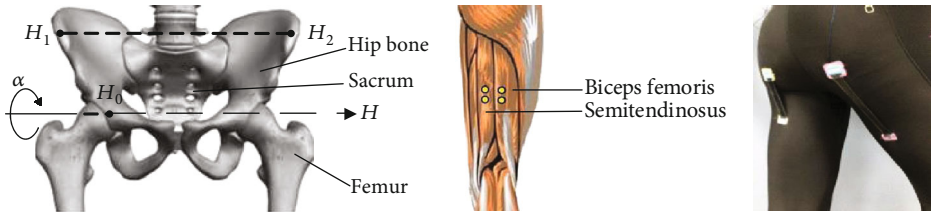

Figure 6: Sensor integrated position analysis of the hip joint.

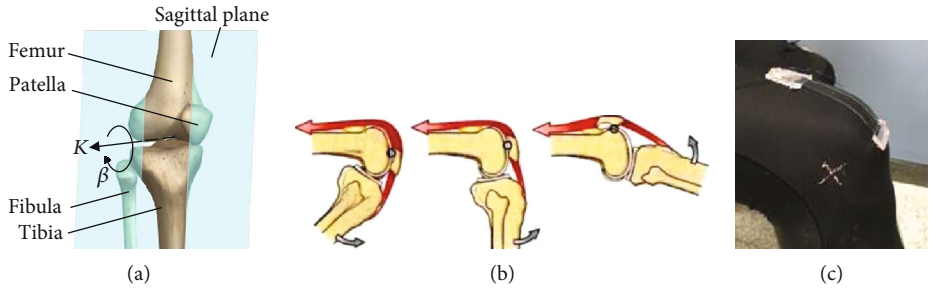

Figure 7: Position analysis of the sensor for knee joint detection.

freedom, namely, flexion/extension, abduction/adduction, and internal/external rotation. According to the International Society of Biomechanics (ISB), the flexion/extension movements in the sagittal plane can be simplified to a hinge mechanism composed of the femur and the hip bone. The H-axis of the hinge motion is required to cross the center point H_0 of the hip joint and parallel to the line formed by points H_1 and H_2 of the anterior superior iliac spine (ASIS) on both sides of the hip; the rotational angle of flexion/-extension movements of the hip is denoted as α as shown in Figure 6(a). The biceps femoris is located on the posterior side of the thigh, which belongs to the posterior muscle groups, as shown in Figure 6(b). The biceps femoris can flex the knee joint and extend the hip joint, which are fundamental movements of the thigh. Therefore, the soft sensor was placed at the biceps femoris, and its two ends were sewn to the pants as shown in Figure 6(c).

The knee joint is composed of the lower end of the femur and the upper end of the tibia and the patella. The flexion/-extension is the primary movement of the knee during gait. According to the ISB general standard, as shown in Figure 7, the flexion/extension movements of the knee joint in the sagittal plane can be simplified to the hinge mechanism composed of the femur, tibia, and fibula. The K-axis of hinge motion is across the motion axis of the knee joint and perpendicular to the sagittal plane. The relative rotation angle of flexion/extension movements is expressed as β, as shown in Figure 7. The ideal position of the sensor on the knee joint is to cover all the patella if the patella only rotates; however, the patella not only rotates but also slides on the femur, as shown in Figure 7(b). Therefore, the better design is covering only half of the patella to obtain a convenient calculation. Specifically, the lower end of the sensor is placed at the middle of patella, and the upper end is located on the quadriceps, as shown in Figure 7(c).

The skeletal structure of the ankle joint consists of the lower end of the fibula and the lower end of the tibia and the talus (Figure 8(a)). The ankle joint has three degrees of freedom, namely, dorsiflexion/plantarflexion, inversion/-eversion, and internal/external rotation. During walking, the ankle joint performs dorsiflexion/plantarflexion movement almost entirely in the sagittal plane, so it can be simplified into a hinge mechanism composed of the lower leg and the foot. According to the ISB general standard, in the coronal plane, the line connecting the inner apex A_2 and the outer apex A_1 is the axis of the ankle joint moving in

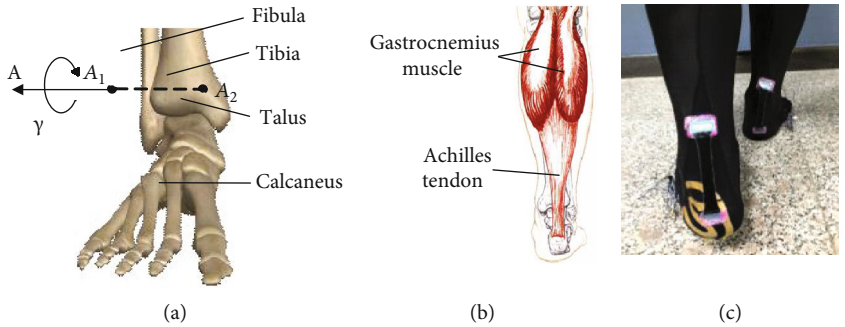

Figure 8: Sensor integrated position analysis of the ankle joint.

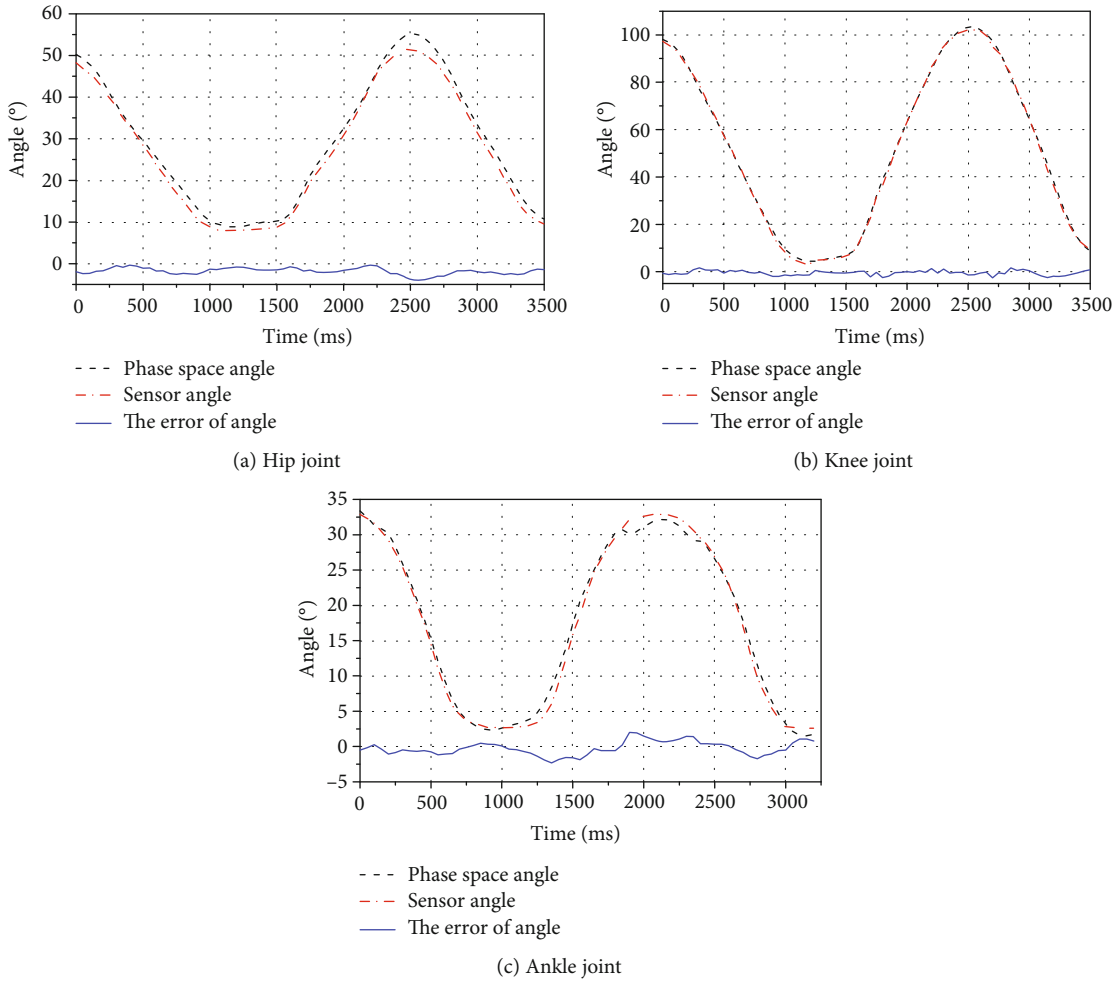

Figure 9: Measurements of the joint motions by utilizing DES and PhaseSpace during squatting with 0.4 Hz.

the sagittal plane. The relative rotation angle of the ankle joint is denoted as γ as shown in Figure 8(a). The Achilles tendon is located between the heel and the lower leg; it would be stretched if the ankle joint performs dorsiflexion/plantarflexion movement. The movement of the Achilles tendon can well reflect the movement of the ankle joint, so a soft sensor for measuring the ankle joint motion can be placed at the Achilles tendon as shown in Figures 8(b) and 8(c).

5. Measurements of Leg Motion by Using the Integrated Wearable Strain Sensor

Typical motions of the leg are squatting and walking; in this experiment, squatting was detected first. In order to test the accuracy of the system proposed in this paper, a popular commercial motion capture system PhaseSpace was employed, and the leg motions were captured by both systems

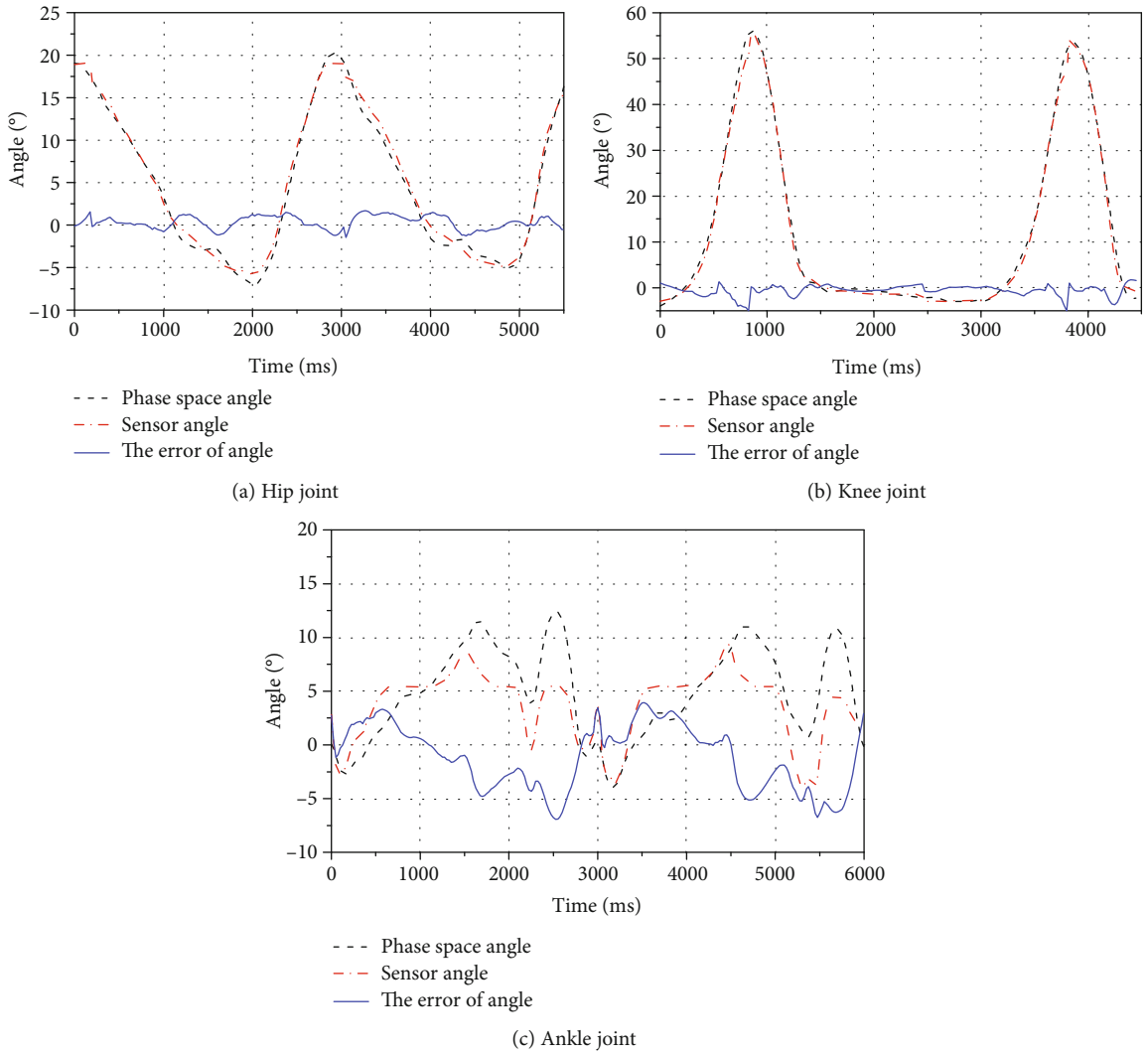

Figure 10: Measurements of the joint motions by utilizing DES and PhaseSpace during walking with a step frequency of 0.33 Hz.

simultaneously. Comparing measurements from both systems, performance of the proposed system can be evaluated. The measurements and the error between them are shown in Figure 9. It can be seen from the data that the dielectric elastomer sensors track the leg motion during squatting and the root-mean-square errors of the joint angles of the hip, knee and ankle are within 3°.

Next, the angles of the joints during walking were measured with a speed of 0.22 m/s, 0.5 m/s, 0.75 m/s, and 1.25 m/s, and the corresponding step frequencies were 0.33 Hz, 0.56 Hz, 0.67 Hz, and 0.83 Hz, respectively. Two sets of experiments were performed for each walking speed, and the root-mean-square error (RMSE) of the join angle measured by DES and PhaseSpace was calculated in each set of experiments. Among them, the comparison between the DES system and PhaseSpace at 0.33 Hz are shown in Figure 10.

There are four groups of measurement data for each joint (two sets of experiments for each leg); by averaging the root-mean-square errors of each joint under the same step frequencies, we can obtain the average root-mean-square errors (RMSE) of each joint at different speeds as shown in Table 3.

As can be seen from Figure 10 and Table 3, the hip and knee joints performed well in the walking test, but the ankle joint performed poorly because the ankle joint has internal/-external rotation and inversion/eversion movement in the nonsagittal plane in order to reduce its motion impact and adjust its center of gravity. To be specific, plantarflexion of the ankle induces internal rotation and inversion; dorsiflexion of ankle induces external rotation and eversion. The movements in nonsagittal planes also influence length variations of the DES, introducing error. However, during a squatting motion, the sole of the foot maintains contact to the ground at all times, limiting the nonsagittal motion of the ankle joint, and thereby reducing the measurement error.

It can be seen from Table 3 that the measurements of the hip joint have varying accuracy at different walking speeds. For the knee joint, if the walking speed does not exceed 0.75 m/s (0.67 Hz), the detection results maintain a high accuracy. However, the detection accuracy decreases when

Table 3: Average root-mean-square errors of motion measurement system under nonsynchronous frequency.

Walking speed (m/s)	Step frequency (Hz)	Average RMSE of hip joint (°)	Average RMSE of knee joint (°)	Average RMSE of ankle joint (°)
0.22	0.33	1.03	1.52	3.42
0.5	0.56	1.38	2.02	3.39
0.75	0.67	1.14	1.92	3.44
1.25	0.83	2.06	4.63	2.60

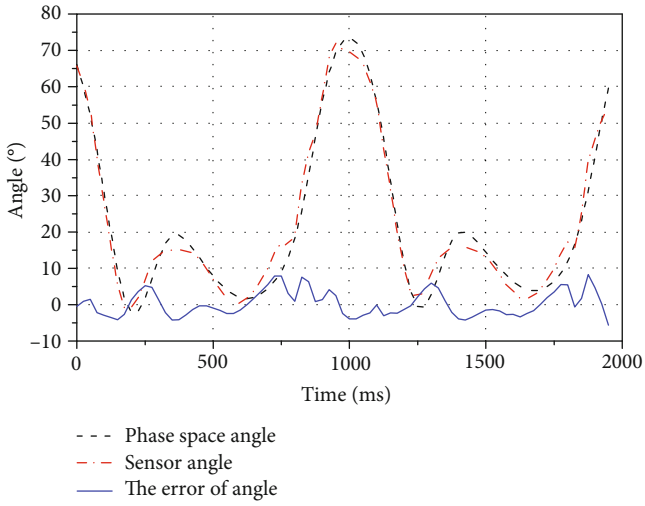

Figure 11: Knee joint test data for walking speed of 1.25 m/s (0.83 Hz).

the walking speed reaches 1.25 m/s; this decrease of accuracy may be from the impact between the leg and the ground. To explain the reason more clearly, data with a walking speed of 1.25 m/s is given in Figure 11, and it can be found that there is an irregular fluctuation when the angle value is at a minimum (when the leg is almost straight). This is because the posture of leg is almost straight when the foot contacts the ground, and the leg adjusts its posture to reduce impact by contacting. The compensation is often to produce a fast flexion and extension movement to extend the duration of the contraction. However, this fast flexion-extension makes a fast elongation-shortening of the DES that introduces a larger measurement error when walking with higher speed. For the ankle joint, the detection is worse than that of the other joints at most walking speeds due to the out-of-plane motion mentioned above. However, measurement accuracy did improve at a speed of 1.25 m/s, which may indicate less out-of-plane coupling at higher walking speeds.

6. Discussion

Compared to commercial motion capture system such as PhaseSpace, the proposed integrated sensing pants is a wearable detection system, and the measurement results can be quickly obtained. The measurement errors of the dynamic detection are better than the published data of dynamic measurements [35–37]. However, there are still some issues that need to be improved. First, the sensors need to be wired into the pants as the wires may influence the reliability and lifetime of the sensors; the best design would be to achieve wireless transmission. Second, the integrated pants with the DES are not very convenient to wear, and it may be better to let the sensors remain independent modules that can be mounted and removed.

In the future, the accuracy of joint rotation can be improved by the following measures: (1) establishing a more precise system model and optimizing relevant parameters to increase the sensitivity of the DES, and (2) measuring the motion in both the sagittal and nonsagittal planes synchronously to limit any influence from coupling.

7. Conclusions

In this paper, we proposed a dynamic measurement system for leg motion based on dielectric elastomer sensors, which can detect squatting with an accuracy of 3° and walking with an accuracy of 5°. The sampling frequency of the system reached 200 Hz. The accuracy and response of the proposed system can meet majority of applications to measure human motion. In order to achieve high detection speed and sensitivity, a circuit system model was established and verified, and the circuit parameters were optimized by using the model. Based on the physiological characteristics of the human body, the characteristics of the hip, knee, and ankle joint movement were analyzed. According to the muscle distribution, the position and posture that are more favorable to the strain of the sensor are found: The hip joint sensor is arranged above the ischial tubercle and biceps femoris; the knee joint sensor is arranged above the patella and the quadriceps femoris; and the ankle joint sensor is arranged above the calcaneus and the Achilles tendon. Finally, the sensor is integrated and packaged with a pair of pants.

The DES is soft, flexible, and customizable, so it can be easily fitted to the surface of the skin and is well-suited to be worn on the human body. This DES system can be applied to rehabilitation training, analysis of athletic performance for training, and virtual reality systems. It can also be integrated into exoskeleton robotic systems to detect joint motions.

Data Availability

The data used to support the findings of this study are included within the article.

Conflicts of Interest

The authors declare no conflict of interest.

Authors' Contributions

Yaqing Feng and Yongze Li designed the DES. David McCoul revised the manuscript. Shihao Qin performed the experiments. Tao Jin improved the system model. Bo Huang improved performance of the sensors. Jianwen Zhao proposed the idea and methods of the measurements. Yaqing Feng and Yongze Li contributed equally to this work.

Acknowledgments

This work was supported by the National Natural Science Foundation of China (Grant No. 91648106) and the Primary Research & Development Plan of Shandong Province (Grant No. 2017GGX10128).

References

[1] H. P. Bruckner, W. Theimer, and H. Blume, "Real-time low latency movement sonification in stroke rehabilitation based on a mobile platform," in *2014 IEEE International Conference on Consumer Electronics (ICCE)*, Las Vegas, NV, USA, 2014.

[2] Y. Cha, K. Nam, and D. Kim, "Patient posture monitoring system based on flexible sensors," *Sensors*, vol. 2017, no. 17, p. 584, 2017.

[3] L. Wang, L. Zheng, K. Jiang, and G. Shen, "Bio-multifunctional smart wearable sensors for medical devices," *Advanced Intelligent Systems*, vol. 5, no. 1, article 1900040, 2019.

[4] S. Noiumkar and S. Tirakoat, "Use of optical motion capture in sports science: a case study of golf swing," in *2013 International Conference on Informatics and Creative Multimedia*, Kuala Lumpur, Malaysia, 2013.

[5] D. K. Arvind and M. M. Bartosik, "Motion capture and classification for real-time interaction with a bipedal robot using on-body, fully wireless, motion capture specknets," in *RO-MAN 2009 - The 18th IEEE International Symposium on Robot and Human Interactive Communication*, Toyama, Japan, 2009.

[6] M. Zhang, "Application of performance motion capture technology in film and television performance animation," *Applied Mechanics and Materials*, vol. 347-350, pp. 2781–2784, 2013.

[7] J. Rebelo, T. Sednaoui, E. B. D. Exter et al., "Bilateral robot teleoperation: a wearable arm exoskeleton featuring an intuitive user interface," *IEEE Robotics & Automation Magazine*, vol. 21, no. 4, pp. 62–69, 2014.

[8] D. M. Vogt and R. J. Wood, "Wrist angle measurements using soft sensors," in *SENSORS, 2014 IEEE*, pp. 1631–1634, Valencia, Spain, November 2014.

[9] M. Mihelj, T. Nef, and R. Riener, "ARMin II—7 DoF rehabilitation robot: mechanics and kinematics," in *Proceedings 2007 IEEE International Conference on Robotics and Automation*, pp. 4120–4125, Roma, Italy, April 2007.

[10] Z. Kadivar, J. L. Sullivan, D. P. Eng et al., "RiceWrist robotic device for upper limb training: feasibility study and case report of two tetraplegic persons with spinal cord injury," *International Journal of Biological Engineering*, vol. 2, no. 4, pp. 27–38, 2012.

[11] D. J. Williams, H. I. Krebs, and N. Hogan, "A robot for wrist rehabilitation," in *2001 Conference Proceedings of the 23rd Annual International Conference of the IEEE Engineering in Medicine and Biology Society*, vol. 2, pp. 1336–1339, Istanbul, Turkey, October 2001.

[12] B. H. Ran and F. Zhang, "Investigation on relative factors of wrist and shoulder injuries in badminton sports," *Chinese Journal of Clinical Rehabilitation*, vol. 10, pp. 41–43, 2006.

[13] A. Pfister, A. M. West, S. Bronner, and J. A. Noah, "Comparative abilities of Microsoft Kinect and Vicon 3D motion capture for gait analysis," *Journal of Medical Engineering & Technology*, vol. 38, no. 5, pp. 274–280, 2014.

[14] D. Vlasic, R. Adelsberger, G. Vannucci et al., "Practical motion capture in everyday surroundings," *ACM Transactions on Graphics*, vol. 26, no. 3, p. 35, 2007.

[15] H. Y. Song, J. G. Zhang, and F. Wang, "Study on motion measurement of human upper limb based on electromagnetic tracking system during the activities of daily living," *Applied Mechanics and Materials*, vol. 321-324, pp. 684–687, 2013.

[16] G. Dudek and M. Jenkin, "Inertial sensors, GPS, and odometry," in *Springer Handbook of Robotics*, B. Siciliano and O. Khatib, Eds., vol. 20, pp. 477–490, Springer, Berlin, Heidelberg, 2008.

[17] D. Roetenberg, H. Luinge, and P. Slycke, "Xsens MVN: full 6DOF human motion tracking using miniature inertial sensors," Tech. Rep. Xsens Motion Technologies BV, 2009.

[18] S. Tadakaluru, W. Thongsuwan, and P. Singjai, "Stretchable and flexible high-strain sensors made using carbon nanotubes and graphite films on natural rubber," *Sensors*, vol. 14, no. 1, pp. 868–876, 2014.

[19] H. Ying, H. Chao, L. Jian et al., "Highly stretchable, rapid-response strain sensor based on SWCNTs/CB nanocomposites coated on rubber/latex polymer for human motion tracking," *Sensor Review*, vol. 39, no. 2, pp. 233–245, 2018.

[20] S. Tadakaluru, T. Kumpika, E. Kantarak et al., "Highly stretchable and sensitive strain sensors using nano-graphene coated natural rubber," *Plastics, Rubber and Composites*, vol. 46, no. 7, pp. 301–305, 2017.

[21] K. Kim, S. Hong, H. Cho et al., "Highly sensitive and stretchable multidimensional strain sensor with prestrained anisotropic metal nanowire percolation networks," *Nano Letters*, vol. 15, no. 8, pp. 5240–5247, 2015.

[22] A. Nag, R. B. V. B. Simorangkir, E. Valentin et al., "A transparent strain sensor based on PDMS-embedded conductive fabric for wearable sensing applications," *IEEE Access*, vol. 6, pp. 71020–71027, 2018.

[23] H. Niu, H. Zhou, H. Wang, and T. Lin, "Polypyrrole-coated PDMS fibrous membrane: flexible strain sensor with distinctive resistance responses at different strain ranges," *Macromolecular Materials Engineering*, vol. 301, no. 6, pp. 707–713, 2016.

[24] X. X. Gong, G. T. Fei, W. B. Fu et al., "Flexible strain sensor with high performance based on PANI/PDMS films," *Organic Electronics*, vol. 47, pp. 51–56, 2017.

[25] Z. Wang, Y. Huang, J. Sun et al., "Polyurethane/cotton/carbon nanotubes core-spun yarn as high reliability stretchable strain sensor for human motion detection," *ACS Applied Materials & Interfaces*, vol. 8, no. 37, pp. 24837–24843, 2016.

[26] J. Xie, H. Long, and M. Miao, "High sensitivity knitted fabric strain sensors," *Smart Materials and Structures*, vol. 25, no. 10, article 105008, 2016.

[27] M. Zhang, C. Wang, H. Wang, M. Jian, X. Hao, and Y. Zhang, "Carbonized cotton fabric for high-performance wearable strain sensors," *Advanced Functional Materials*, vol. 27, no. 2, article 1604795, 2017.

[28] J.-H. Kong, N.-S. Jang, S.-H. Kim, and J. M. Kim, "Simple and rapid micropatterning of conductive carbon composites and its application to elastic strain sensors," *Carbon*, vol. 77, pp. 199–207, 2014.

[29] M. Amjadi, A. Pichitpajongkit, S. Lee, S. Ryu, and I. Park, "Highly stretchable and sensitive strain sensor based on silver nanowire–elastomer nanocomposite," *ACS Nano*, vol. 8, no. 5, pp. 5154–5163, 2014.

[30] F. Pan, S. M. Chen, Y. Li et al., "3D graphene films enable simultaneously high sensitivity and large stretchability for strain sensors," *Advanced Functional Materials*, vol. 28, no. 40, article 1803221, 2018.

[31] B. Huang, M. Li, T. Mei et al., "Wearable stretch sensors for motion measurement of the wrist joint based on dielectric elastomers," *Sensors*, vol. 17, no. 12, p. 2708, 2017.

[32] T. A. Gisby, B. M. O'Brien, and I. A. Anderson, "Self sensing feedback for dielectric elastomer actuators," *Applied Physics Letters*, vol. 102, article 193703, 2013.

[33] D. Xu, T. G. Mckay, S. Michel, and I. A. Anderson, "Enabling large scale capacitive sensing for dielectric elastomers," in *Electroactive Polymer Actuators and Devices (EAPAD) 2014*, vol. 9056, p. 90561A, San Diego, CA, USA, 2014.

[34] D. Xu, A. Tairych, and I. A. Anderson, "Stretch not flex: programmable rubber keyboard," *Smart Materials and Structures*, vol. 25, no. 1, article 015012, 2015.

[35] C. R. Walker and I. A. Anderson, "Monitoring diver kinematics with dielectric elastomer sensors," in *Electroactive Polymer Actuators and Devices (EAPAD) 2017*, vol. 10163, p. 1016307, Portland, Oregon, USA, 2017.

[36] Y. Mengüç, Y. L. Park, H. Pei et al., "Wearable soft sensing suit for human gait measurement," *The International Journal of Robotics Research*, vol. 33, no. 14, pp. 1748–1764, 2014.

[37] X. Ma, J. Guo, K. M. Lee, L. Yang, and M. Chen, "A soft capacitive wearable sensing system for lower-limb motion monitoring," in *International Conference on Intelligent Robotics and Applications. ICIRA 2019*, H. Yu, J. Liu, L. Liu, Z. Ju, Y. Liu, and D. Zhou, Eds., vol. 11743 of Lecture Notes in Computer Science, pp. 467–479, Springer, Cham, 2019.

[38] B. O'Brien, I. Anderson, E. Calius, E. Haemmerle, and S. Xie, "Integrated extension sensor based on resistance and voltage measurement for a dielectric elastomer," in *Electroactive Polymer Actuators and Devices (EAPAD) 2007*, San Diego, CA, USA, 2007.